Revolutionizing lung cancer detection using hybrid CNN-LSTM (HCLSTM) for accurate diagnosis and enhanced nodule classification

Lavanya Mathiyalagi A.[a,*], R. Ravi[b]

[a] *Assistant Professor, Information Technology, PSN Engineering College, Tirunelveli- 627451, Tamil Nadu, India*
[b] *Professor, Computer Science and Engineering, Francis Xavier Engineering College, Tirunelveli 627003 Tamil Nadu, India*

ARTICLE INFO

ABSTRACT

This paper presents a strong lung cancer detection and classification system that combines state-of-the-art image processing, feature extraction, optimization, and deep learning to promote diagnostic precision. Gaussian filters and morphological transformations are applied in the pre-processing phase to remove noise and improve the visibility of lung nodule edges, while histogram equalization is applied for normalization of brightness to make the tumor clearly visible. Gray-Level Co-occurrence Matrix (GLCM) and Principal Component Analysis (PCA) capture and filter texture-based features to establish a meaningful and compact feature set. Enhanced Reptile Predator Optimization (IRPO) algorithm selects highly related features without being stuck in local optima and optimizing parameter tuning. Last but not least, the Hybrid Convolutional Long Short-Term Memory (HCLSTM) network combines CNN and LSTM layers to obtain correct classification by maintaining spatial and temporal patterns. The novel strategy achieved 98.45 % accuracy, 98.21 % precision, 98.60 % recall, and 98.40 % F1-score on the IQ-OTH/NCCD lung cancer dataset, better than the existing state-of-the-art techniques. Such findings reflect the applicability of the introduced framework to support early diagnosis and personalized treatment planning in clinical settings.

1. Introduction

Lung cancer is one of the leading causes of cancer-related death across the world, accounting for the largest number of cancer cases and deaths every year. According to recent statistics, lung cancer is accountable for causing an estimated 1.8 million new cases and more than 600,000 fatalities annually, with high rates of incidence being most predominantly apparent in nations like the United States [1,2]. Despite ongoing advancements in medical science, lung cancer is a daunting task due to its delayed rate of detection and low survival rate [3,4]. Asymptomatic early lung cancer has been discovered to be responsible for late diagnosis following progression of the disease, thereby limiting the therapeutic interventions and the chances of effective treatment [5]. Accurate and early detection therefore becomes essential to enhance patient survival, facilitate early interventions, and healthcare cost savings due to the management of advanced disease [6]. Lung cancer most often occurs as a result of mutations in lung cell DNA, which results in uncontrolled cell growth and cancer development [7]. Its etiology is determined by an interaction of genetic predispositions with exposures to environmental and lifestyle factors. Tobacco smoking, radon gas exposure, asbestos, and other environmental toxins are major risk factors [8]. Its complex and multifactorial etiology makes it even more challenging to achieve early and accurate diagnosis. Thus, it is a pressing requirement for emerging diagnostic approaches that might make early detection possible, decrease misdiagnosis, and enable individualized treatment protocols [9,10].

The routine diagnostic methods, such as chest X-rays, computed tomography (CT), positron emission tomography (PET) scanning, bronchoscopy, and tissue biopsies, have all been the old standard against lung cancer [11]. Of these, CT scans especially low-dose CT (LDCT) have emerged as the first choice in screening for high-risk patients because they are capable of picking up very small tumor sizes and abnormal growths [12]. The tests, however, are not without flaw. They tend to be interpretation-dependent, may need specialized knowledge, are observer-variable, and may cause false positives or negatives. It is these limitations that are the cause of unnecessary invasive diagnostic tests, delayed diagnosis, or missed malignancies [13]. To reduce this, computer-aided diagnosis (CAD) systems have come into prominence as potential tools that can help increase detection accuracy, offer standardized assessment, and aid decision-making in clinicians. CAD

systems employ sophisticated image processing algorithms and machine learning parameters for lung image pre-processing, identification of useful features, and discrimination of benign and malignant nodules [14]. Fuzzy c-means clustering and k-means clustering, edge detection, and optimization algorithms like particle swarm optimization and genetic algorithms have been used to enhance feature extraction and segmentation [15]. Deep learning models, particularly convolutional neural networks (CNNs) like AlexNet, VGG-16, and LeNet, have further advanced the field by enabling automated analysis of large and complex image datasets with high precision.

This paper presents its main contributions through the following sections:

- This work enhances the pre-processing pipeline: It introduces Gaussian filters, morphological operations, and histogram equalization to reduce noise, sharpen lung nodule edges, and improve tumor visibility, thereby aiding in more accurate diagnostics.
- This work establishes robust feature extraction: By applying GLCM for texture analysis and PCA for dimensionality reduction, it generates a feature set that captures essential lung nodule characteristics.
- Through its feature selection approach this work uses IRPO to find key predictive features which enhances the performance and decreases the computational needs of the classification model.
- Under this work, researchers created a hybrid classification model which integrates spatial processing from CNN alongside temporal analysis from LSTM in the HCLSTM model for accurate benign and malignant nodule differentiation.

This paper contains the following sections as the main parts of the content. The part 2 section contains both related works and the problem statement. The Section 3 demonstrates the implementation of the proposed method. The paper provides results in part 4 along with discussions which lead to the result presented in part 5.

2. Literature review

Researchers explored the benefits of merging FFBPNN with SVM to enhance lung cancer classification accuracy during 2021 according to Nanglia et al. [16]. Utilizing a dataset of 500 images (75 % for training, 25 % for testing), the study introduces a three-block mechanism: data preprocessing, feature extraction using the SURF technique with Genetic Algorithm optimization, and final classification via FFBPNN.

A computationally efficient diagnosis system for early detection of these cancers was developed by Mehmood et al. in 2022 [17]. A dataset containing 25,000 images of lung and colon histopathology with five classes enabled an AlexNet model to demonstrate 89 % initial accuracy. To address an underperforming class, targeted contrast enhancement was applied, improving overall accuracy to 98.4 % without compromising computational efficiency.

The research team of Khan et al. [18] introduced a new design for lung cancer analysis through the combination of contrast stretching and feature fusion techniques in 2020. The CT image contrast becomes enhanced through gamma correction. The system combines various extracted features through canonical correlation analysis. The ensemble classifier achieves better classification outcomes by combining critical features that result from entropy-based filtering and weighted NCA application.

During 2020 Manoharan conducted research about automated breast cancer detection through image analysis and CPU-based data malignancy evaluations [19]. A modified image processing filter inside the proposed algorithm helps select nodule features alongside a neural classifier that lowers false positive mistakes. Research results validated the diagnostic accuracy of the model by generating response characteristic curves when it was implemented for internal and external nodule cancer diagnosis.

The study published by Han et al. [20] during 2021 evaluated PET/ CT image capabilities to identify different NSCLC histologic types while investigating the most effective ML and DL model for radiomics analysis. The research team examined 867 adenocarcinoma (ADC) patients and 552 squamous cell carcinoma (SCC) cases based on retrospective data analysis followed by testing on 283 patients and training the rest. The research extracted 688 features that were evaluated alongside ten feature selection methods as well as ten ML models and the VGG16 DL algorithm.

In 2023, Varchagall *et al.* [21] used machine learning to determine tumorous lung characteristics on CT scans. Although a 3D ResNet model learned emphysema with an AUC of 0.79, it initially showed limited success with opacity and cancer. Transfer learning was applied to improve results, achieving comparable outcomes for emphysema and opacities. This classification could help predict health complications related to cancer spread.

In 2023, Gite *et al.* [22] highlighted the novelty of using U-Net++ for lung segmentation in X-rays, presenting a comprehensive comparison with three benchmark architectures. The authors demonstrate that U-Net++ surpasses traditional U-Net in accuracy and mean Intersection over Union (IoU), achieving over 98 % lung segmentation accuracy and a mean IoU of 0.95, thereby minimizing data leakage in TB diagnosis.

The research group of Harsono et al. [23] created I3DR-Net as a new lung nodule detection and classification system during 2022 to address crucial diagnosis challenges of lung malignancy which ranks as a top global cause of death. Radiologists who operate medical imaging systems must analyze numerous images yet they must prioritize quality above quantity due to excessive image exposure. The diagnostic process becomes inaccurate due to misinterpretations which primarily occur when medical personnel analyze ambiguous partially enlarged lymph nodes. This leads to worse detection accuracy and sensitivity of malignant nodules. The I3DR-Net system brings together an Infected 3D ConvNet (I3D) pre-trained backbone architecture and a feature pyramid network which optimizes 3D CT scan dataset analysis across multiple scales.

A new method from Tiwari et al. [24] in 2023 merges Gaussian filters with RNN-GAN architecture for lung tumor detection purposes. The RNN tracks temporal sequences within image data followed by GAN implementation which improves training by generating artificial tumor samples. Advantageous application of a Gaussian filter obtains better quality images and enables better feature extraction.

The researchers at Fu et al. [25] advanced in 2021 a PET-CT architecture for cancer examination which integrated the tumor-detecting characteristics of PET with CT's anatomical capabilities. The current automated segmentation methods show limitations because they demand intensive expert manual input that leads to errors. Our proposed deep learning technique uses a multimodal spatial attention module (MSAM) to focus on tumor scan areas in PET while minimizing normal tissue display.

While previous studies have introduced various approaches for lung cancer detection, significant performance and methodological gaps remain. For instance, Mehmood et al. achieved 89 % initial accuracy using an AlexNet model on histopathology images, which was later improved to 98.4 % through targeted contrast enhancement. However, this method required additional preprocessing steps to compensate for class imbalance and struggled with certain underrepresented classes. Similarly, Khan et al. combined contrast stretching with feature fusion and canonical correlation analysis, but their ensemble classifier relied on extensive handcrafted feature engineering, limiting scalability and adaptability across diverse datasets. Recent deep learning models, such as 3D ResNet and U-Net++ have shown promise, yet they primarily focus on segmentation or single-modality classification without integrated optimization of feature selection and temporal-spatial patterns. The I3DR-Net improved multi-scale analysis but did not incorporate feature selection mechanisms to reduce computational load or address high-dimensional feature redundancy.

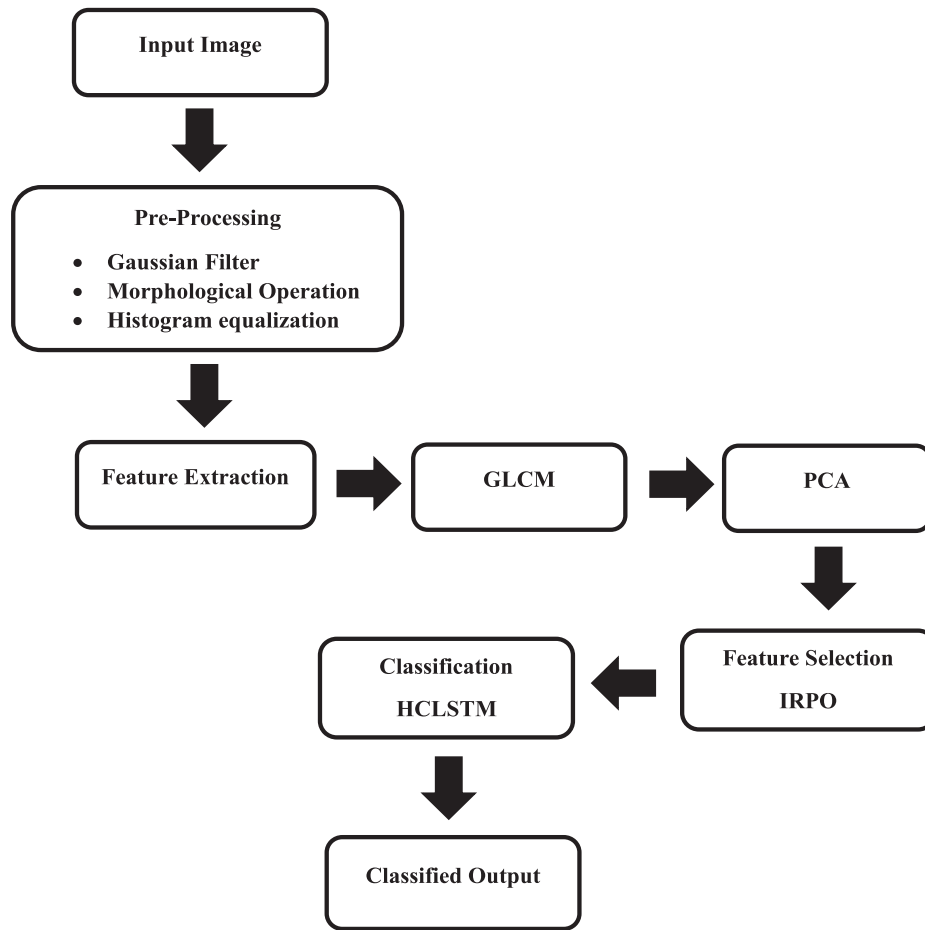In contrast, this study introduces several unique contributions that

Fig. 1. Overall proposed methodology.

address these gaps:

- This work proposed the use of Improved Red Panda Optimization (IRPO) for feature selection, which identifies the most predictive features while reducing computational demands a step often missing in prior deep learning-based CAD systems.
- This work designed a hybrid classification model (HCLSTM) that integrates the spatial processing power of CNNs with the temporal sequence analysis strength of LSTMs, enabling superior benign-versus-malignant nodule differentiation.
- This method achieves improved diagnostic accuracy while lowering false positives/negatives, offering an integrated pipeline from noise reduction to classification without requiring excessive manual intervention or multiple optimization stages.
- This approach directly overcomes the limitations in prior work by enhancing feature robustness, reducing dimensionality effectively, and combining spatial–temporal analysis in a single framework to support precise and early lung cancer diagnosis.

2.1. Problem statement

The process of early lung cancer detection proves challenging because initial symptoms from early stages are both numerous and minimal which leads to late diagnosis and restricted therapeutic options. The diagnostic methods of traditional X-rays and CT scans show weak abilities to analyze between malignant and benign lung nodules because they possess low precision and accuracy levels. Using these methods may produce numerous incorrect positive results thus triggering

expensive and uncomfortable biopsy procedures that present health threats. The detection process becomes difficult because of complex lung tissue arrangements together with imaging noise. The standard imaging evaluation method fails to detect small or unobtrusive nodules which delays proper medical diagnosis. Early detection of malignant cells needs reliable detection techniques that would improve survival rates because it is extremely important to have such methods in place right now. Lung cancer detection requires developed techniques which deliver precise diagnosis without harm to patients and at early disease stages because they improve patient results while cutting healthcare expenses.

3. Proposed methodology

Diagnosing lung cancer has critical importance due to its fatal outcome while various factors such as imaging noise alongside unclear boundaries and excessive false-positive citations make accurate diagnosis difficult. This research implements state-of-the-art image preprocessing methods that include Gaussian filtering along with morphological process to enhance nodule edge definition and apply histogram equalization for brightness normalization to improve nodule detection. The method extracts crucial features by applying the GLCM technique for texture analysis and using PCA to reduce dimensions which produces a compact yet informative feature collection. IRPO recognizes the best predictive factors that the HCLSTM employs to provide precise nodule diagnoses that contribute to quicker treatments.

3.1. Pre-processing

Gaussian filtering and morphological processing for image quality enhancement enable this work to be of superior quality, and histogram equalization provides even brightness for better visualization of nodules. Preprocessing Gaussian filtering and morphological processing enhance detection of nodules significantly by eliminating noise and enhancing image contrast, making boundary delineation clear, enabling more accurate feature extraction. Results indicate that incorporation of these steps enhanced detection accuracy and decreased false positives, which directly affected the model's overall performance and validity.

3.1.1. Gaussian filtering

Gaussian filtering is a fast-smoothing function in image processing used for the reduction of noise since it operates to maintain important edge structures. It performs a weighted mathematical process between pixels that are neighboring using a Gaussian function involving calculations of central pixel distances. Central pixel weight is more than neighbor pixels due to which it forms a smooth gradient that eliminates sudden changes in pixel intensity but retains meaningful outline detail. Degree of smoothing is controlled through the sigma (σ) parameter of Gaussian function width adjustments that controls the lens-like extent of blur effect. Gaussian filter of sigma = 1.5 was chosen after trial to get the best compromise between noise removal and edge preservation. This choice ensures that small nodules remain visible while background noise is effectively suppressed, facilitating more accurate segmentation. Additionally, the filter's radius or size determines the extent of weighted averaging, effectively setting the neighborhood over which the filter operates. Gaussian filtering is especially useful for removing Gaussian noise and is favoured over basic mean filtering because it better preserves edges and finer details. Its performance in isotropic smoothing tasks is improved by its non-causal character, which ensures that smoothing is symmetrical in all directions. The system's general architecture is shown in Fig. 1.

3.1.2. Morphological operations

Morphological operations are methods of image processing that concentrate on examining and manipulating the form and structure of objects in an image. Although grayscale photos can also be employed, binary images are the main target of these processes. Morphological procedures are mostly used to improve features, remove noise, or extract significant structures from an image. Erosion, dilatation, opening, and shutting are important processes.

• Erosion

Image processing through morphological operations focuses on analyzing as well as modifying structural and shape characteristics of image components. The main objects of these processes consist of binary images even though grayscale photos can serve as suitable alternatives. Morphological procedures mainly serve two purposes: structure extraction and feature improvement and noise removal within images. The major operations are erosion followed by dilatation and opening and closing.

• Dilation

Expansion of objects in binary images is done by dilation through the addition of pixels to their boundary areas. As with any morphological operation, the aforementioned utilizes an element that scans the entire image. Properness of position of output pixels to foreground occurs when any pixel of the structuring element aligns with background pixels (white pixels). The output pixel is white whenever anyone pixel of the structuring element coincides with the image foreground. By dilation the process joins two nearby objects and fills in small gaps and enlarges their dimensions.

• Opening

A binary image uses opening as a morphological process that removes small noise elements without damaging greater objects' overall form and dimension. The entire process involves doing erosion followed by dilation. In dilation the process returns big surviving objects to their previous size and retains noise-free structures. Erosion does the opposite, contracting small objects first before eliminating the noise. Two-stage cleansing process safeguards useful image structures and properly eliminates the noise from the image through this operation.

• Closing

A binary image benefits from closing when it performs morphological operations to fill small holes within object boundaries. The first stage applies dilation then erosion to execute this operation. The enlarging aspect of the structuring element performs dilation on foreground items to fill all small openings in the image pattern. Small gaps located after dilation become eliminated through the erosion process without modifying the object dimensions. The closure process boosts image form structuring by filling small spaces and by making objects more connected.

3.1.3. Histogram equalization

The technique for image processing called histogram equalization modifies image contrast by readjusting pixel intensity values. The brightness distribution receives adjustments through this process for creating more balanced pixel intensity distributions. Application of this process expands the image dynamic range to show details concealed in dark and light areas.

Steps for histogram equalization

• Calculate Histogram: The image requires histogram creation through pixel intensity level count establishment.
• Compute Cumulative Distribution Function (CDF): Compute the running sum of histogram values, normalizing it to form the CDF.
• Normalize Intensities: Multiply the CDF values by the maximum grayscale value (e.g., 255 for an 8-bit image), and round the results to the nearest integer.
• Map Original Intensities: Replace each pixel's intensity in the authentic image with its comparable value from the equalized CDF.

The result is an image with enhanced contrast. Although the new histogram isn't perfectly flat, it's closer to uniform, which makes the image's features more visible across varying lighting conditions.

3.2. Feature extraction

In this study, GLCM analyzes texture features, while PCA reduces data dimensions, creating a compact feature set for lung cancer detection.

3.2.1. GLCM

GLCM examines image textures through its ability to detect pixel value relations that result from grayscale conversion. The extraction of spatial features happens through a kernel process that produces a matrix specific to texture details. In the analysis, contrast, homogeneity, energy, and correlation are the four primary aspects.

Contrast: Contrast measurements are essential to the spatial frequency analysis of an image. In GLCM analyses, the contrast analysis quantifies the difference between the most and least significant pixel values. Greater variations within the local texture of the image are indicated by higher contrast levels. This feature uses Eq. (1).

Homogeneity: The inverse variation moment calculation measures the distribution uniformity of GLCM elements. The feature detects close-diagonal elements while its values grow when visual image objects share

similarities. Uniform textures correspond to high homogeneity values in quantitative analysis. This feature is using Eq. (2).

Energy: The image energy measurement finds its value through calculating the square root of angular second moment data which describes the pixel pair consistency. Higher energy levels equate to more ordered distribution of pixel pairings, which results in more textual consistency. This functionality makes use of Equation (3).

Correlation: This technique may be used to quantify the degree of linear correlation between image grayscale values. The measurement assesses the connection of pixel brightness values over the whole image. The degree of pixel value correlation reveals texture consistency through elevated values of correlation measured in linear fashion. This feature is using Eq. (4).

$$contrast = \sum_{i=0}^{B-1} \sum_{j=0}^{B-1} (i-j)^2 \tag{1}$$

$$homogeneity = \sum_{i=0}^{B-1} \sum_{j=0}^{B-1} \frac{Z(i,j)}{1+(i-j)^2} \tag{2}$$

$$energy = \sqrt{\sum_{i=0}^{B-1} \sum_{j=0}^{B-1} Z(i,j)^2} \tag{3}$$

$$correlation = \sum_{i=0}^{B-1} \sum_{j=0}^{B-1} \frac{(i-\mu_i)(j-\mu_j)}{\sqrt{(\sigma_i)(\sigma_j)}} \tag{4}$$

Position (i,j) within the kernel contains its normalized gray-scale value as indicated byZ(i,j) and B represents the gray level total. This procedure ensures the overall value sums to 1. The extraction of textural features from grayscale images relied on rotations at four angles: 0°, 45°, 90° and 135° for every analyzed feature.

3.2.2. PCA

PCA functions as a statistical approach to reduce data dimensions while executing data compression tasks. The data transformation process through PCA reduces high-dimensional features to lower dimensions by maintaining most essential information while identifying directions of maximum data variation. PCA uses linear combinations of original features to create orthogonal components which represent the principal factors of the data set. Data analysis through covariance matrix eigenvalue and eigenvector calculation produces these components. PCA transforms the original data while the eigenvectors form the principal components and each eigenvalue indicates the corresponding variance. The covariance matrix eigenvalues and vectors determine principal components from which PCA derives data projections. The projection operation maintains the complete variability existing in the original input data. This is a basic description of PCA.

1. Covariance matrix calculation

Given a dataset X with n observations and p features, calculate the covariance matrix C is expressed as per Eq. (5).

$$C = \frac{1}{n-1}(X - \overline{X})^T (X - \overline{X}) \tag{5}$$

2. Eigenvalue decomposition

As per Eq. (6), compute the eigenvalues $(\lambda_1, \lambda_2, \cdots, \lambda_p)$ and corresponding eigenvectors $(v_1, v_2, \cdots, v_p)$ of the covariance matrix C.

$$Cv_i = \lambda_i v_i \tag{6}$$

3. Sort eigenvalues

Sort the eigenvalues in descending order and reconstruct the corresponding eigenvectors accordingly.

4. Select principal components

Choose the first k eigenvectors corresponding to the k largest eigenvalues to form the transformation matrix M.

5. Project data

The transformed dataset Y results from projecting original data X onto the new subspace that M defines. PCA maintains high data variance as it performs dimension reduction. PCA determines main directional components which explain the maximum data variability and utilizes them to reduce the dimensions while retaining essential information.

3.3. Feature selection

In this work, IRPO algorithm identifies the most predictive features, optimizing data input for enhanced classification model performance.

3.3.1. IRPO

Red panda, which has reddish-brown fur and characteristic markings, occurs in southern China and eastern Himalayas. The species inhabits temperate forests with dense bamboo cover, where it exhibits impressive tree-climbing ability. The animal applies its sharp senses and tree-climbing ability to survive by feeding on bamboo shoots and leaves. Red Panda Optimization (RPO) was created based on the inspiration of red pandas' natural behavior.

IRPO algorithm was employed to select the best 20 features from the extracted set to be utilized within this study. Features were of primary significance in enabling correct lung nodule classification. Generally, the selected features were primarily texture-related (e.g., entropy, contrast, homogeneity), shape-related (e.g., compactness, sphericity), and edge smoothness-related (e.g., gradient-based edge sharpness, boundary regularity). These characteristics were observed to be important in distinguishing between malignant and benign nodules.

Mathematical modelling
Initialization
The RPO method implements red pandas as symbolic representations for the individual members in its population-based metaheuristic algorithm. Every red panda from the population serves as a potential solution that exists within the search area. The positions of these red pandas are initialized randomly to explore the search space effectively. The red panda's position is represented mathematically as a vector, forming a population matrix Y. This matrix is initialized using Eq. (7) and Eq. (8):

$$X = \begin{bmatrix} X_1 \\ \cdot \\ \cdot \\ X_i \\ \cdot \\ \cdot \\ X_M \end{bmatrix}_{M \times n} = \begin{bmatrix} X_{1,1} \cdots X_{1,j} \cdots X_{1,n} \\ \cdot \\ \cdot \\ X_{i,1} \cdots X_{i,j} \cdots X_{i,n} \\ \cdot \\ \cdot \\ X_{M,1} \cdots X_{M,j} \cdots X_{M,n} \end{bmatrix}_{M \times n} \tag{7}$$

$$x_{i,j} = lob_j + r_{i,j} \bullet \left(upb_j - lob_j \right), \quad i = 1, M, j = 1, n \tag{8}$$

The objective function values of the initialized solutions are evaluated and represented as per Eq. (9).

$$f = \begin{bmatrix} f_1 \\ . \\ . \\ . \\ f_i \\ . \\ . \\ f_M \end{bmatrix}_{M \times 1} = \begin{bmatrix} f(X_1) \\ . \\ . \\ . \\ f(X_i) \\ . \\ . \\ f(X_M) \end{bmatrix}_{M \times 1} \quad (9)$$

where, f_i is the objective function value for the i-th red panda. These values help evaluate the quality of potential solutions, identifying the best and worst solutions to guide the optimization process.

Phase 1: exploration strategy: foraging

Red pandas use certain positional movements to follow their innate food-searching behavior during the initial stage of RPO. They use their keen senses to gravitate toward food. The algorithm's red pandas look at other participants' superior objective function value locations as possible food sources. Red pandas use Eq. (10), which compares objective function values, to randomly choose their suggested food locations.

$$pfs_i = \{X_k | k \in \{1, 2, .., M\} and f_k < f_i \} \cup \{X_{best}\} \quad (10)$$

Determination of new locations relative to the food source by red pandas through best candidate solution demonstrates similarities to the foraging behaviour of these animals. Eq. (11) to Eq. The red panda's new position can be calculated using Eq. (13) when the objective function shows enhanced results in its current location.

$$X_i^{p1} : x_{i,j}^{p1} = x_{i,j} + r.\left(sfs_{i,j} - Is.y_{i,j}\right) + x_i' \quad (11)$$

$$x_i' = X_i + \Delta X_i \quad (12)$$

$$X_i = \begin{cases} X_i^{p1}, f_i^{p1} < f_i \\ X_i, else \end{cases} \quad (13)$$

Gaussian mutation balances exploration and exploitation by adjusting the standard deviation. It's simple to implement and adaptable, with mutation strength decreasing over time to enhance convergence in optimization algorithms.

Phase 2: expertise in climbing and perching on trees

The second part of the RPO simulates the resting and tree-climbing activities of red pandas. After scouring the ground, red pandas use these arboreal environments to get food, which is why they wander between tree branches. This manipulation helps RPO boost its exploration of suitable problem regions and local search techniques simultaneously due to slight alterations in its position. The model of tree-climbing behavior computes new red panda positions which substitute past positions when the objective function results in improvement according to Eqs. (14) and (15):

$$X_{i,j}^{p2} = x_{i,j} + \frac{lob_j + r_{i,j} \bullet \left(upb_j - lob_j\right)}{t}, \quad i = 1, 2, \cdots, M, j = 1, 2, \cdots, n, t$$
$$= 1, 2, \cdots, T \quad (14)$$

$$X_i = \begin{cases} X_i^{p2}, & f_i^{p2} < f_i \\ X_i, & else \end{cases} \quad (15)$$

The iterative counter of the algorithm is represented by t and T signifies the maximum allowed iterations. Positional refinement of red pandas increases optimization efficiency and directs the algorithm to find optimal solutions during this stage.

3.4. Classification

This research incorporates HCLSTM to perform spatial CNN feature extraction along with LSTM temporal processing for exact lung nodule classification.

3.4.1. HCLSTM

CNN operates as a deep learning model that excels at uncovering key patterns from image-based raw data through its learning capabilities. The four layers that compose CNN networks consist of Convolutional followed by pooling and activation functions before reaching the fully connected layer to generate an output. Features in images become extracted through filters which are used in convolutional layers while pooling layers reduce the size of extracted features. The combination of activation functions along with fully connected layers forms a predictive mechanism in CNN models. At the same time the models undergo training they learn optimal parameter settings via backpropagation together with gradient descent methods while regulate Cyclic training enables CNN models to develop better skills for image object identification and classification. The solution of long-term assurance in sequential input required Long Short-Term Memory (LSTM) versions of recurrent neural networks (RNN) for its resolution. The memory blocks in these networks enable continuous information storage thus making them highly adequate for dealing with time-series data as well as natural language processing tasks.

The HCLSTM architecture integrates convolutional and recurrent layers to effectively capture both spatial and temporal features from input data. The CNN component consists of two convolutional layers: the first with 64 filters, a 3 × 3 kernel size, stride 1, and ReLU activation, followed by batch normalization and a 2 × 2 max pooling layer; the second convolutional layer uses 128 filters, a 3 × 3 kernel, ReLU activation, batch normalization, and 2 × 2 max pooling. These convolutional layers extract high-level spatial features. The output is then passed to a bidirectional LSTM layer with 128 units, which captures sequential dependencies in both forward and backward directions. Dropout with a rate of 0.5 is applied to prevent overfitting. Following the LSTM, a fully connected dense layer with 64 units and ReLU activation is used, and the final output layer employs softmax activation for classification. The model is trained using the Adam optimizer with a learning rate of 0.001, categorical cross-entropy loss, batch size of 32, and for 50 epochs. L2 regularization is applied to the dense layers to improve generalization. This detailed configuration ensures the architecture can be accurately reproduced for further study or comparison.

- Input Layer: Receives sequential data input.
- Hidden Layer: Contains LSTM units responsible for processing and retaining information.
- Output Layer: The system generates the finished output after information processing.

LSTM replaces the basic units of regular RNNs with memory cells, which allow them to retain information over long sequences. LSTM units have three main gates: input gate, forget gate, and output gate.

- Input Gate: coordinate how fresh data enters the memory cell.
- Forget Gate: Selects the data from the memory cell to remove.
- Output Gate: Adjusts the output according to the input's previous state and present value.

The activation of each LSTM unit at time l_t is calculated using Eq. (16):

$$l_t = \sigma(wm_{i,l} \bullet x_t + wm_{h,l} \bullet l_{t-1} + bi) \quad (16)$$

where, l_t and l_{t-1} represent the activation at time respectively, σ is a nonlinear activation function, $wm_{i,l}$ is the input-hidden weight matrix, $wm_{h,l}$ is the hidden-hidden weight matrix, bi is the hidden bias vector, and x_t is the input at time t. LSTM networks excel at grasping long-term dependencies in sequential data. They mitigate the problem of gradient vanishing, allowing for more effective learning over longer sequences.
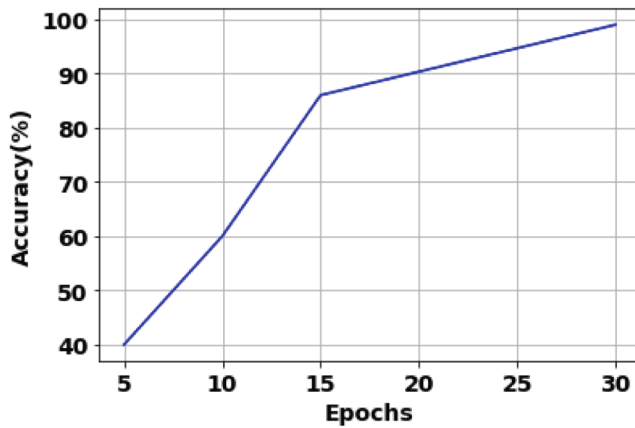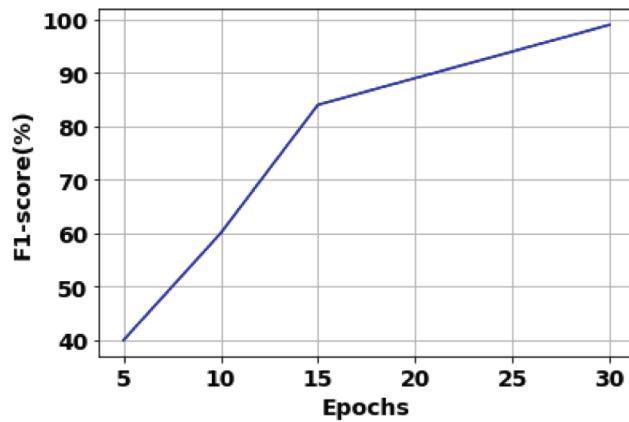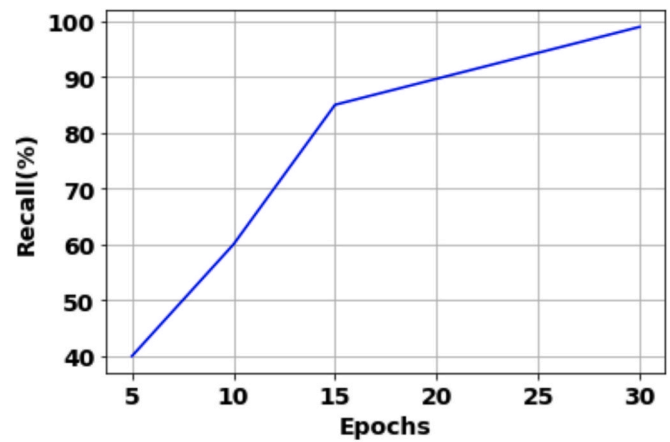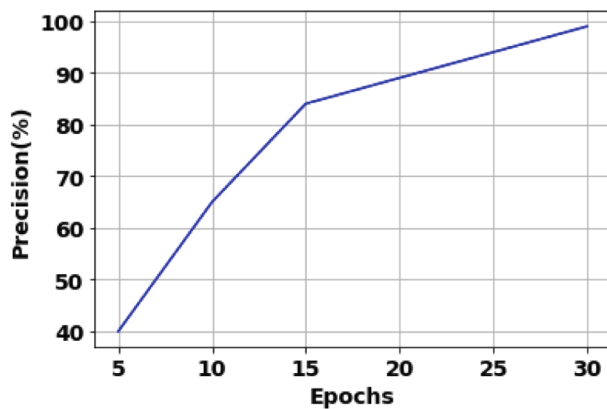
Fig. 2. Performance metrics by varying epochs.

4. Result and discussion

The Python-based implementation of the proposed HCLSTM framework demonstrates substantial improvements in detecting and accurately classifying cancerous cells. The chosen performance metrics accuracy, precision, recall, and F1-score achieved impressive values during both training and testing phases. Specifically, the proposed method attained 98.45 % accuracy, 98.21 % precision, 98.60 % recall, and 98.40 % F1-score on the IQ-OTH/NCCD lung cancer dataset. These results outperform existing approaches, confirming the superior

effectiveness of the integrated IRPO-HCLSTM framework in lung cancer classification.

4.1. Dataset collection

This IQ-OTH/NCCD Lung Cancer Dataset [26] data set contains 110 patient CT scan images treated at Iraq-Oncology Teaching Hospital/ National Center for Cancer Diseases in 2019. The data set contains three individual groupings distinguishing normal and benign from malignant outcomes. The images are 1190 total including 40 malignancies and 15
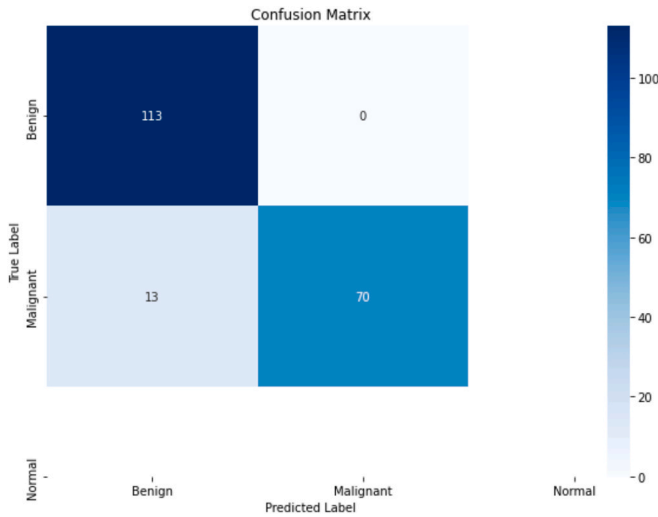
Fig. 3. Confusion matrix.

significantly as the epochs increase, eventually stabilizing at a high level. This trend indicates that the model converges well with more training cycles, achieving a consistent and reliable performance due to the IRPO's enhanced optimization capabilities. By effectively searching through the solution space, IRPO avoids local minima, leading to better parameter tuning for the HCLSTM model.

In Fig. 3, the confusion matrix shows that the model accurately classifies the majority of test samples with minimal misclassifications. The high values along the diagonal reflect the model's strong ability to correctly distinguish between normal, benign, and malignant cases, confirming its effectiveness in multi-class classification.

In Fig. 4, it displays the pre-processed images, highlighting the initial enhancements applied before feeding the images into the model. These pre-processing steps contribute to clearer features for the HCLSTM to learn. Fig. 5 shows the predicted images, which closely match the ground truth. The precise predictions illustrate the model's robustness in feature extraction and pattern recognition. In Fig. 6, the histogram graph depicts the pixel intensity distribution before and after processing, showcasing a more balanced and enhanced intensity range post-equalization. This histogram adjustment improves the visibility of image details, aiding the HCLSTM in better feature learning.
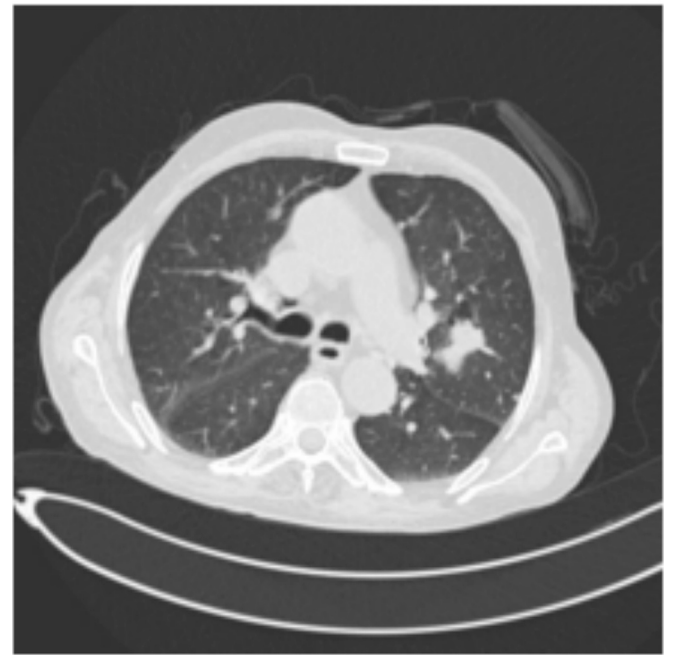
benign cases along with 55 normal cases. The Siemens SOMATOM scanners obtained the images at a slice thickness of 1 mm, and there is no patient information in the data to ensure anonymity. The dataset is normally utilized by researchers to perform research on lung cancer recognition algorithms and classification methods.

The IQ-OTH/NCCD Lung Cancer Dataset was split into training, validation, and testing subsets for accurate model assessment. The dataset was exactly 70 % allocated to training, 15 % to validation, and 15 % to testing. Splitting was stratified in order to maintain the class distribution between normal, benign, and malignancy cases in each subset. Furthermore, the five-fold cross-validation approach was applied in training to enhance the HCLSTM model's ability to generalize and prevent overfitting. The model performance indicators reported are the mean over the cross-validation folds with final testing on the independent test set.

To avoid possible overfitting because of the limited dataset, methods like 5-fold cross-validation, dropout, L2 regularization, and early stopping were used. Data augmentation (scaling, rotation, flipping) helped in increasing sample diversity, but the model generalized more. All these measures helped the model generalize well on both the training and validation sets.

4.2. Analysis of performance

The results conferred in Figs. 2–6 highlight the performance of the model using IRPO and HCLSTM, demonstrating the convincingness of these methods in enhancing classification accuracy and image prediction quality.

In Fig. 2, the graph illustrates the model's accuracy, precision, recall, and F1-score across different epochs. The performance metrics improve

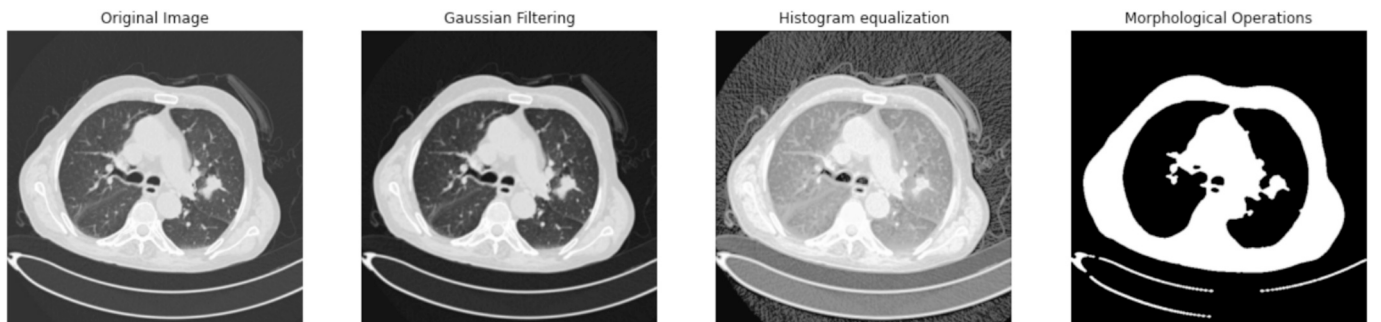

Fig. 5. Predicted image.

Fig. 4. Pre-processed images.
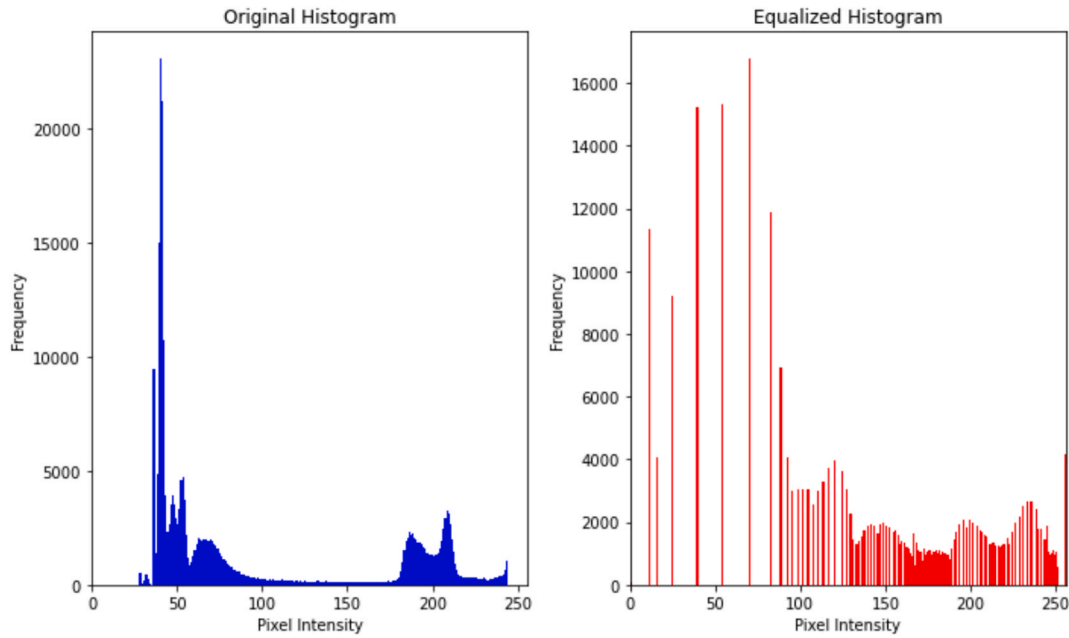
Fig. 6. Histogram graph.

Table 1
Existing model comparison.

Model	Accuracy (%)	Precision (%)	Recall (%)	F1-Score (%)
CNN	93.75	93.10	94.00	93.55
LSTM	92.85	92.00	93.50	92.75
CNN-LSTM (without IRPO)	95.60	95.30	95.80	95.55
Proposed IRPO-HCLSTM	98.45	98.21	98.60	98.40

4.3. Comparison with existing methods

To further validate the effectiveness of the proposed IRPO-HCLSTM framework, its performance was compared against other state-of-the-art models, including traditional CNN, standalone LSTM, and a CNN-LSTM hybrid without IRPO optimization. Table 1 summarizes the comparative results on the same dataset.

As seen in Table 1, the proposed IRPO-HCLSTM outperformed all comparison models across all performance metrics. The integration of IRPO significantly contributed to optimizing hyperparameters and avoiding local minima, leading to superior parameter tuning. Additionally, the hierarchical structure of HCLSTM enabled the effective capture of both spatial and temporal features, which enhanced classification accuracy.

4.4. Error analysis and model limitations

Although the proposed HCLSTM framework achieved high performance across all key metrics, certain limitations were observed during the evaluation:

Misclassification of Borderline Cases: The confusion matrix (Fig. 3) reveals that a small number of benign nodules were misclassified as malignant, particularly in cases where nodule texture or shape closely resembled malignant patterns. This highlights the challenge in distinguishing subtle variations between benign and malignant features.

Sensitivity to Image Quality: While pre-processing improved image clarity, the model's accuracy slightly decreased when presented with low-contrast or partially obscured CT images. This suggests that the model's robustness may be affected by poor image quality or artifacts introduced during scanning.

Dataset Imbalance Effect: The dataset contains fewer benign instances than malignant and normal classes. Even when optimization methods have been applied, such imbalance may have influenced negligible classification bias, as evidenced in rather worse precision for the benign class.

Generalization to External Datasets: The model has been validated on the IQ-OTH/NCCD dataset. Its performance on other datasets or in real-world multi-center clinical settings remains to be explored. Domain adaptation or transfer learning strategies might be required for broader applicability.

Addressing these limitations will be the focus of future work, where additional data augmentation, ensemble learning, and domain adaptation techniques could further enhance model robustness and generalizability.

5. Conclusion

Researchers established an advanced imaging technique with processing methods for diagnosing lung cancer more precisely while reducing the number of inaccurate positives detected. The pre-processing stage applied Gaussian filters together with morphological operations to decrease noise and make lung nodules have sharper edges. The application of Histogram equalization enabled the study to normalize picture brightness so tumors became more detectable. The research used GLCM for texture analysis combined with PCA for feature extraction where the techniques generated an information-rich feature set. The IRPO methodology selected optimal predictive characteristics that supported the classification model input stage. The HCLSTM network containing LSTM and CNN elements was employed in classification model operations. The hybrid detection model served as a promising screening method because it successfully identified different types of pulmonary nodules. The proposed method stands to improve patient results substantially through its capability to generate early interventions and patient-specific treatment programs.

Future work could focus on expanding this framework by incorporating larger and more diverse datasets to further validate the model's robustness and generalizability. In addition, fine-tuning the HCLSTM parameters or exploring alternative deep learning architectures may

lead to further performance gains. The framework could also be extended to other cancer types such as breast cancer or brain tumors to evaluate its adaptability across different medical imaging challenges.

Consent to participate

Not applicable.

Consent for publication

Not applicable.

Human and animal ethics

Not applicable.

Code availability

Not applicable.

Author's contributions

Author 1: Performed the Analysis the overall concept, writing and editing.

Author 2: Participated in the methodology, Conceptualization, Data collection and writing the study.

CRediT authorship contribution statement

A. Lavanya Mathiyalagi: Writing – review & editing, Writing – original draft. **R. Ravi:** Formal analysis, Data curation.

Ethics approval

No ethics approval is required.

Funding

On Behalf of all authors the corresponding author states that they did not receive any funds for this project.

Declaration of competing interest

The authors declare that they have no known competing financial interests or personal relationships that could have appeared to influence the work reported in this paper.

Data availability

All the data is collected from the simulation reports of the software and tools used by the authors. Authors are working on implementing the same using real world data with appropriate permissions.

References

[1] A. Heidari, D. Javaheri, S. Toumaj, N.J. Navimipour, M. Rezaei, M. Unal, A new lung cancer detection method based on the chest CT images using Federated Learning and blockchain systems, Artif. Intell. Med. 141 (2023) 102572.
[2] Z. Shen, P. Cao, J. Yang, O.R. Zaiane, WS-LungNet: a two-stage weakly-supervised lung cancer detection and diagnosis network, Comput. Biol. Med. 154 (2023) 106587.
[3] B. Ar, V.K. Rs, K. Ss, LCD-capsule network for the detection and classification of lung cancer on computed tomography images, Multimed. Tools Appl. 82 (24) (2023) 37573–37592.
[4] D. Lu, Z. Shangguan, Z. Su, C. Lin, Z. Huang, H. Xie, Artificial intelligence-based plasma exosome label-free SERS profiling strategy for early lung cancer detection, Anal. Bioanal. Chem. 416 (23) (2024) 5089–5096.
[5] R. de Vries, N. Farzan, T. Fabius, F.H. De Jongh, P.M. Jak, E.G. Haarman, E. Snoey, J. CCM, Y.W. Dagelet, A.H. Maitland-Van Der Zee, A. Lucas, Prospective detection of early lung cancer in patients with COPD in regular care by electronic nose analysis of exhaled breath, Chest 164 (5) (2023) 1315–1324.
[6] F. Ahmad, U. Hariharan, S. Karthick, V.E. Pawar, S. Sharon Priya, Optimized lung nodule prediction model for lung cancer using contour features extraction, Opt. Mem. Neural Networks 32 (2) (2023) 126–136.
[7] R. Raza, F. Zulfiqar, M.O. Khan, M. Arif, A. Alvi, M.A. Iftikhar, T. Alam, Lung-EffNet: lung cancer classification using EfficientNet from CT-scan images, Eng. Appl. Artif. Intel. 126 (2023) 106902.
[8] U. Subashchandrabose, R. John, U.V. Anbazhagu, V.K. Venkatesan, M. Thyluru Ramakrishna, Ensemble Federated learning approach for diagnostics of multi-order lung cancer, Diagnostics 13 (19) (2023) 3053.
[9] S. Srivastava, N. Jayaswal, S. Kumar, P.K. Sharma, T. Behl, A. Khalid, S. Mohan, A. Najmi, K. Zoghebi, H.A. Alhazmi, Unveiling the potential of proteomic and genetic signatures for precision therapeutics in lung cancer management, Cell. Signal. 113 (2024) 110932.
[10] Y. Yao, Z. Li, Y. Han, L. Xie, X. Zhao, Z. Zhu, Fabrication and characterization of a MnO2/Ti3C2Tx based gas sensor for highly sensitive and selective detection of lung cancer marker hexanal, Chem. Eng. J. 451 (2023) 139029.
[11] M.H. Sabzalian, F. Kharajinezhadian, A. Tajally, R. Reihanisaransari, H. A. Alkhazaleh, D. Bokov, New bidirectional recurrent neural network optimized by improved Ebola search optimization algorithm for lung cancer diagnosis, Biomed. Signal Process. Control 84 (2023) 104965.
[12] R. Mothkur, B.N. Veerappa, Classification of lung cancer using lightweight deep neural networks, Proc. Comput. Sci. 218 (2023) 1869–1877.
[13] A. Forder, R. Zhuang, V.G. Souza, L.J. Brockley, M.E. Pewarchuk, N. Telkar, G. L. Stewart, K. Benard, E.A. Marshall, P.P. Reis, W.L. Lam, Mechanisms contributing to the comorbidity of COPD and lung cancer, Int. J. Mol. Sci. 24 (3) (2023) 2859.
[14] X. Cheng, X. Xia, D. Ren, Q. Chen, G. Xu, F. Wei, J. Yang, L. Wang, Q. Hu, J. Zou, Y. Cen, Programmable CRISPR-Cas12a and self-recruiting crRNA assisted dual biosensing platform for simultaneous detection of lung cancer biomarkers hOGG1 and FEN1, Anal. Chim. Acta 1240 (2023) 340748.
[15] K.S. Pradhan, P. Chawla, R. Tiwari, HRDEL: High ranking deep ensemble learning-based lung cancer diagnosis model, Expert Syst. Appl. 213 (2023) 118956.
[16] P. Nanglia, S. Kumar, A.N. Mahajan, P. Singh, D. Rathee, A hybrid algorithm for lung cancer classification using SVM and Neural Networks, ICT Express 7 (3) (2021) 335–341.
[17] S. Mehmood, T.M. Ghazal, M.A. Khan, M. Zubair, M.T. Naseem, T. Faiz, M. Ahmad, Malignancy detection in lung and colon histopathology images using transfer learning with class selective image processing, IEEE Access 10 (2022) 25657–25668.
[18] M.A. Khan, S. Rubab, A. Kashif, M.I. Sharif, N. Muhammad, J.H. Shah, Y.D. Zhang, S.C. Satapathy, Lung's cancer classification from CT images: an integrated design of contrast based classical features fusion and selection, Pattern Recogn. Lett. 129 (2020) 77–85.
[19] S. Manoharan, Early diagnosis of lung cancer with probability of malignancy calculation and automatic segmentation of lung CT scan images, J. Innov. Image Process. 2 (04) (2020) 175–186.
[20] Y. Han, Y. Ma, Z. Wu, F. Zhang, D. Zheng, X. Liu, L. Tao, Z. Liang, Z. Yang, X. Li, J. Huang, Histologic subtype classification of non-small cell lung cancer using PET/CT images, Eur. J. Nucl. Med. Mol. Imaging 48 (2021) 350–360.
[21] M. Varchagall, N.P. Nethravathi, R. Chandramma, N. Nagashree, S.M. Athreya, Using deep learning techniques to evaluate lung cancer using CT images, SN Comput. Sci. 4 (2) (2023) 173.
[22] S. Gite, A. Mishra, K. Kotecha, Enhanced lung image segmentation using deep learning, Neural Comput. Appl. 35 (31) (2023) 22839–22853.
[23] I.W. Harsono, S. Liawatimena, T.W. Cenggoro, Lung nodule detection and classification from Thorax CT-scan using RetinaNet with transfer learning, J. King Saud Univ.-Comput. Inf. Sci. 34 (3) (2022) 567–577.
[24] A. Tiwari, S.A. Hannan, R. Pinnamaneni, A.R.M. Al-Ansari, Y.A.B. El-Ebiary, S. Prema, R. Manikandan, Optimized ensemble of hybrid rnn-gan models for accurate and automated lung tumour detection from ct images, Int. J. Adv. Comput. Sci. Appl. 14 (7) (2023).
[25] X. Fu, L. Bi, A. Kumar, M. Fulham, J. Kim, Multimodal spatial attention module for targeting multimodal PET-CT lung tumor segmentation, IEEE J. Biomed. Health Inform. 25 (9) (2021) 3507–3516.
[26] Dataset taken from: "https://www.kaggle.com/datasets/adityamahimkar/iqoth nccd-lung-cancer-dataset", dated 1/10/2024.